Technical Note: Cumulative Dose Modeling for Organ Motion Management in MRI-Guided Radiation Therapy

Seyed Ali Mirzapour

Department of Industrial, Systems, and Manufacturing Engineering, Wichita State University, Wichita, KS, 67260, USA

Thomas R. Mazur

Department of Radiation Oncology, Washington University in St. Louis, St. Louis, MO, 63110, USA

H. Harold Li

Department of Radiation Oncology, Washington University in St. Louis, St. Louis, MO, 63110, USA

Ehsan Salari

Department of Industrial, Systems, and Manufacturing Engineering, Wichita State University, Wichita, KS, 67260, USA

Gregory C. Sharp [a)]

Department of Radiation Oncology, Massachusetts General Hospital, Boston, MA, 02114, USA

(Dated: 18 September 2020)

[a)] Author to whom correspondence should be addressed. Electronic mail: gcsharp@mgh.harvard.edu. Mailing address: Department of Radiation Oncology, Massachusetts General Hospital, 55 Fruit Street, Boston, MA 02114.

Purpose: To develop a method for continuous on-line dose accumulation during irradiation in MRI-guided radiation therapy (MRgRT), and to demonstrate its application in evaluating the impact of internal organ motion on cumulative dose.

Methods: An intensity-modulated radiation therapy (IMRT) treatment plan is partitioned into its unique apertures. Dose for each planned aperture is calculated using Monte Carlo dose simulation on each phase of a four-dimensional computed tomography (4D-CT) dataset. Deformable image registration is then performed both (i) between each frame of a cine-MRI acquisition obtained during treatment and a reference frame and (ii) between each volume of the 4D-CT phases and a reference phase. These registrations are used to associate each cine image with a 4D-CT phase. Additionally, for each 4D-CT phase, the deformation vector field (DVF) is used to warp the pre-calculated dose volumes per aperture onto the reference CT dataset. To estimate the dose volume delivered during each frame of the cine-MRI acquisition, we retrieve the pre-calculated warped dose volume for the delivered aperture on the associated 4D-CT phase and adjust it by a rigid translation to account for baseline drift and instances where motion on the cine image exceeds the amplitude observed between 4D-CT phases.

Results: The proposed dose accumulation method is retrospectively applied to a liver cancer case previously treated on an MRgRT platform. Cumulative dose estimated for free-breathing and respiration-gated delivery is compared against dose calculated on static anatomy. In this sample case, the target minimum dose and D_{98} varied by as much as 5% and 7%, respectively.

Conclusion: We demonstrate a technique suitable for continuous on-line dose accumulation during MRgRT. In contrast to other approaches, dose is pre-calculated per aperture and phase and then retrieved based on a mapping scheme between cine MRI and 4D-CT datasets, aiming at reducing the computational burden for potential real-time applications.

Keywords: organ motion modeling, MRI guidance, radiotherapy

I. INTRODUCTION

Respiratory motion can induce large tumor displacement and organ deformation particularly in thoracic and abdominal cancers by as much as 2 centimeters (cm)[1,2]. Various strategies exist in radiotherapy planning for managing respiratory motion. For example, an internal target volume (ITV) can be defined to include the entire motion envelope inferred during simulation CT. While ITV-based approaches mitigate the likelihood of geometric misses, treated volumes can be much larger than the gross tumor volume (GTV) itself and treatments can be susceptible to interplay effects. Gating is an alternative motion management strategy that interrupts treatment whenever the target moves beyond an allowed threshold. Through gating, target volumes can be reduced at the expense of treatment efficiency. On conventional linear accelerators (linacs), tumor motion is evaluated via surrogates such as implanted fiducial markers or a patient's surface. More recently, MRgRT delivery platforms have enabled gating via direct tumor tracking on planar, cine images acquired during treatment.

More sophisticated motion management strategies attempt to achieve the advantages of both ITV-based treatment and gating. For example, MLC tracking shifts the leaf trajectory of a modulated treatment according to a patient's respiratory motion. Using MLC tracking, treatment can, in principle, be delivered to the clinical target volume (CTV) without compromising duty cycle. Various motion surrogates have been demonstrated for application to MLC tracking including fiducial markers and electromagnetic transponders. A variant of MLC tracking is tumor trailing, where the leaf sequence in an IMRT treatment is offset to compensate for baseline drift. Cine imaging in MRgRT provides direct imaging of tumor motion that can support a robust implementation of these techniques.

Methods such as MLC tracking and tumor trailing are examples of feedforward control where a disturbance (i.e., patient motion) is measured and a compensating action (i.e., shifting of MLC leaves) is applied to preserve system performance (i.e., delivery of planned dose to CTV). Ongoing advancements in intra-fractional imaging for MRgRT delivery systems provide the opportunity to implement closed-loop feedback control, where the compensating action can be adjusted while monitoring system performance in real time to achieve an optimal dosimetric result in terms of both tumor targeting and normal-tissue sparing. To achieve such feedback in this context, a necessary prerequisite is a tool for accurate, intra-fractional dose accumulation that can be implemented in real time for comparing doses delivered to different structures to planned or clinically desired

values.

Various dose accumulation techniques have been described, mostly for retrospective evaluation of delivered dose. The simplest approaches model motion as shifts applied to a planned dose distribution and estimate cumulative dose through convolution of the static dose with a distribution of shifts[3–5]. While well-suited for fast calculation, these approaches can compromise accuracy specifically in heterogeneous conditions and in the presence of large deformations. More realistic approaches compute dose per position and aperture. Varying degrees of complexity have been investigated for these approaches. For instance, Poulsen et al.[6] described a technique for evaluating interplay effects that modeled motion by rigid isocenter shifts. By re-calculating dose per aperture to a plan with these shifts applied, an estimate for composite dose could be realized. More recently, Stemkens et al.[7] proposed a more advanced approach that applies Monte Carlo calculation per aperture to pseudo-CT data generated via motion models. While arguably providing the most physically realistic estimates for accumulated dose, this approach presents computational hindrances for real-time application.

In this note, we outline a dose accumulation approach that combines aspects of previously described methods to potentially achieve sufficiently accurate intra-fractional dose accumulation in real time for closed-loop feedback in MRgRT. The described approach combines 4D-CT images acquired at the time of CT simulation with planar, cine-MRI acquisition during treatment. The framework for dose accumulation is defined prior to treatment by (i) performing deformable image registration between 4D-CT phases and a reference CT; and (ii) calculating dose per aperture for a given plan on each 4D-CT phase and warping it to the reference CT. Then during treatment each cine-MRI frame is associated to a 4D-CT volume with, if needed, an offset correction. Dose at a given instant can then be retrieved and added to a static frame-of-reference given the delivered aperture, associated 4D-CT with offset, and per aperture warped dose.

The novelty of the proposed dose accumulation method lies in its compromise between computational effort and dosimetric accuracy in order to support real-time dose accumulation. A key advantage of the proposed approach is that all dose calculation is performed prior to treatment and intra-fractional dose accumulation is achieved by employing a novel anatomic mapping scheme between cine-MRI frames and 4D-CT motion phases. As a proof-of-principle illustration, we apply this approach to a liver cancer case treated on an MRgRT platform. We specifically compare cumulative dose obtained both for respiration-gated and free-breathing delivery against the planned dose.

II. MATERIALS AND METHODS

Prior to treatment, dose is calculated for each beam aperture on each phase within a 4D-CT acquired at the time of CT simulation. Each 4D-CT phase is deformably registered to a reference CT dataset, which serves as the frame-of-reference for dose accumulation. The pre-calculated dose volumes per aperture and 4D-CT phase are warped using the DVFs. During treatment, each cine-MRI image is associated with one of the 4D-CT phases. Next, the pre-computed warped dose volume corresponding to the current aperture and associated 4D-CT phase is retrieved for accumulation. An additional translation can be applied to correct for deviations in breathing characteristics between 4D-CT and cine MRI. Figure 1 outlines the proposed approach for dose accumulation.

A. Pre-processing Step

Prior to treatment, each 4D-CT phase is deformably registered to the reference CT via performing b-spline registration using the open-source *Plastimatch* software[8]. The reference volume in this study was chosen to be a phase within the 4D-CT acquisition corresponding to end-of-exhalation. Registration was performed using native 4D-CT images with control-point spacing of 30 mm and 20 maximum iteration per stage. To generate 4D-CT motion traces, a region of interest is contoured on the sagittal slice of the reference CT that corresponds to the sagittal plane of the cine-MRI acquisition. Then for each 4D-CT volume, average superior-inferior (SI) displacement of the DVF within the contoured region of interest was extracted. In this study, the region of interest contains the contoured GTV. Additionally, the end-of-exhalation phase is chosen as the phase with the superior-most amplitude for the region-of-interest contour among all 4D-CT phases. Similarly, end-of-exhalation in a breathing cycle on cine MRI is identified by frames with the maximum amplitude in that cycle.

Dose calculation per aperture and 4D-CT phase is performed using an in-house GPU-accelerated Monte Carlo platform that was developed for quality assurance of online adaptive therapy treatments[9]. This platform, gPENELOPE, was developed for a first-generation MRgRT system based on a 0.35 T MRI scanner with three Co-60 sources spaced by 120 degrees on an annular gantry[10]. For each dose calculation, sufficient histories were considered to achieve $< 2\%$ statistical uncertainty in the regions where dose is greater than 50% of maximum dose with isotropic 3 mm resolution. All calculations were performed with a fixed exposure time corresponding to

the imaging frequency such that doses retrieved for accumulation require no further scaling. The obtained dose volumes were warped to the reference CT using *Plastimatch* by applying the DVFs for the associated 4D-CT phases.

B. Anatomic Mapping

The best-matching 4D-CT phase for each cine-MRI image is found based on similarity of the motion in the tracked region of interest (e.g., GTV). On the MRgRT system considered in this note, cine images are acquired throughout treatment in a fixed sagittal plane at four frames per second. Images are acquired using a balanced steady-state free precession sequence with 3.5 mm in-plane resolution and 7 mm slice thickness. The imaging plane is selected to intersect the GTV. Onboard the clinical system, images are deformably registered to a "keyframe" corresponding to a reference image at end-of-exhalation via an intensity-based registration technique[11]. For demonstration of the proposed approach, deformable registration is performed offline using a b-spline technique provided by *Plastimatch* between each image and a representative frame selected at end-of-exhalation. Registration was performed on native images with control point spacing of 14 mm, regularization of 0.1, and 11 maximum iterations per stage.

For each registration, similarly to the 4D-CT volumes, the average SI component of the DVF within the GTV as drawn on the reference cine frame was extracted. A surrogate motion signal is then obtained by constructing a time series consisting of a sequence of amplitude readings at equally-spaced points in time, denoted by $\{x_t : t \in T\}$, where the time step depends on the acquisition rate of the cine-MRI frames. Prior to comparing surrogate signals extracted from DVFs corresponding to 4D-CT and cine-MRI datasets, the cine-MRI motion signal is detrended and adjusted for baseline drift as described later in this section. The adjusted signal, denoted by $\left\{x_t^D : t \in T\right\}$, is then labeled by 4D-CT phases based on amplitude and breathing state at each time step. *Inhale* and *exhale* are distinguished by the sign of the moving average of velocity of the signal ($\bar{v}_t$). More specifically, inhale and exhale correspond to decreasing and increasing components of the motion signal where $\bar{v}_t \leq 0$ and $\bar{v}_t \geq 0$, respectively. Each cine-MRI frame is thus mapped to the best-matching 4D-CT amplitude bin according to the detrended signal amplitude (x_t^D) at that time step and the corresponding breathing stage (i.e., inhale versus exhale). The workflow of the proposed method is shown in Figure 2.

Given that the 4D-CT only captures a rendering of a representative respiratory cycle, some mo-

tion discrepancy between 4D-CT and cine MRI should be expected (e.g., when a patient takes a deeper breath than what might have been captured at CT simulation). Other studies have reported such discrepancy and have generally reported a larger superior-inferior motion range in cine MRI compared to 4D-CT[12]. To account for this potential discrepancy, we apply two rigid corrections to the pre-calculated dose volume at each time step based on comparison between the 4D-CT and cine-MRI surrogate motion signals. First, a baseline shift at time step t, denoted by θ_t^1, is calculated as the difference between the moving average of the peak amplitudes at end-of-exhalation measured over the previous n time steps and the peak amplitude at end-of-exhalation in 4D-CT, as illustrated in Figure 3(a). The calculated value for baseline shift (θ_t^1) is also used to detrend the signal as discussed earlier in this section. Second, it may be possible that the range of the detrended cine-MRI signal in some breathing cycles exceeds that of the 4D-CT signal as shown in Figure 3(b). In such cases, for every time step with an amplitude beyond the 4D-CT range, an out-of-range correction, denoted by θ_t^2, is calculated as the difference between the detrended cine-MRI amplitude and the minimum (maximum) inhalation (exhalation) amplitude on 4D-CT signal. At each time step, we therefore rigidly adjust the dose volume by an offset $\theta_t = \theta_t^1 + \theta_t^2$.

C. Dose Accumulation

Consider a treatment plan consisting of a set of apertures indexed by $a \in \mathcal{A}$. Given the order in which those apertures are delivered as well as their corresponding exposure times, a time series of the sequence of apertures delivered at each time step can be given by $\{a_t : t \in T\}$. To estimate the dose volume delivered at time step t, we first identify the best-matching 4D-CT phase, denoted by ϕ_t, to the acquired cine-MRI frame using the anatomic mapping method described in Section II B. Then the pre-calculated warped dose volume for aperture a_t and 4D-CT phase ϕ_t, denoted by $\mathbf{d}_{(a_t,\phi_t)}$, is retrieved and rigidly adjusted by an offset to account for baseline shift and out-of-range motion. The resulting dose volume, denoted by $\bar{\mathbf{d}}_{(a_t,\phi_t)}$, is then added to the cumulative dose volume. Algorithm 1 shows the pseudo code of the overall dose accumulation procedure.

D. Patient Case

The performance of the proposed dose model was tested on three fractions of a liver cancer case treated on the MRIdian system. The tumor was prescribed to receive 50 Gy in five fractions.

The treatment plan including all unique MLC-defined apertures with associated exposure times (given activity of the Co-60 sources), cine-MRI and 4D-CT images, and associated contours were collected for testing of the proposed technique. The plan in this case consisted of 120 unique apertures spanning seven gantry angles. With ten phases in the 4D-CT, 1200 unique dose calculations were performed for potential retrieval during accumulation.

In the absence of ground truth data, the proposed approach is applied to compare respiration-gated and free-breathing delivery against static anatomy (i.e. the native plan). The clinical treatment was planned on end-of-exhalation and thus for the case of static anatomy the clinical plan was evaluated on the selected reference phase of the 4D-CT. In free-breathing delivery, the treatment is continuously delivered without interruption, while in gated delivery the beam is interrupted depending on tumor position relative to its expected location. In practice on the MRIdian system, gating is achieved by tracking the GTV position on cine-MRI imaging and calculating its fractional area beyond a specified boundary. When this fractional area exceeds a user-specified threshold, the Co-60 sources are retracted and treatment is interrupted until the target is suitably contained within the boundary. For this clinical treatment, gating was applied with a 5% threshold and the boundary was defined by a 3 mm expansion of the GTV.

Given that this case was gated, delivery time per aperture was extracted from a delivery record that provides beam on and off timing. By synchronizing the delivery record to the cine-MRI acquisition, the accumulation procedure in the gating case was ensured to be applied to cine frames for which the beam was on. In the free-breathing case, the procedure was applied to all images in the acquisition up to the total beam-on time indicated by the delivery record. To compare resulting dose distributions, dose-volume histograms (DVHs) were computed for the CTV and the organs at-risk. CTV coverage was evaluated by D_{98} and D_{min} corresponding to minimum dose covering 98% of the CTV and minimum dose delivered to the CTV, respectively. Additionally, D_{mean} (the mean dose) in uninvolved liver and kidneys was evaluated.

III. RESULTS

A. Motion Signal and Phase Labeling

Figure 4(a) exemplifies the motion signal extracted from the cine-MRI images. The motion range of the 4D-CT phases in the SI direction is 9.4 mm, and the average motion range across

the three fractions for the cine-MRI data is 12.3 mm. The red line in Figure 4(a) exemplifies the moving average of the peak amplitudes at end-of-exhalation over an interval of n=50 time steps (12.5 s), which is used to measure the baseline shift. For the displayed region, a maximum baseline drift of approximately 2 mm is evident. The median, maximum, and interquartile range of baseline drift across all fractions are 1.6 mm, 4.5 mm, and 0.7 mm, respectively. Figures 4(b) and 4(c) show the histograms of the baseline-shift and out-of-range corrections, respectively. As can be seen from the two histograms, the magnitude of the baseline shift is relatively larger than the out-of-range correction. Specifically, for the liver case tested in this study, the magnitude of the out-of-range corrections applied to the dose distributions is primarily within 0.5 mm.

Figure 5(a) represents the histogram of the SI displacements obtained from the detrended motion signal for fraction 1 of the liver case. The median and interquartile range of the SI displacements are -1.5 mm and 3.2 mm, respectively. Additionally, Figure 5(b) shows the histogram of the 4D-CT phase labels assigned to the cine-MRI acquisition in fraction 1 by applying the anatomic mapping procedure, as discussed in Section II B. More than 70% of the SI displacements in the motion signal are smaller than 3 mm, which are labeled by either the reference 4D-CT phase 60 or 4D-CT phases close to the reference phase (i.e., 4D-CT phases 30–70). Furthermore, around 10% of the SI displacements are larger than 6 mm; which are labeled by 4D-CT phases 0, 10, or 90. Therefore, a relatively small fraction of the SI displacements are labeled by 4D-CT phases 0, 10, and 90.

B. Dose Aggregation Results

Figure 6 compares the DVH of the planned dose for fraction 1 against the cumulative dose estimated using the proposed method under the respiration-gated and free-breathing deliveries. Additionally, DVH metrics for all three fractions are listed in Table I. The results show that the target coverage under the free-breathing scenario has considerably deteriorated relative to the planned dose (static anatomy) while the respiration-gated scenario achieves a similar target coverage to the planned dose. Under a free-breathing scenario, CTV D_{98} and D_{min} are 8.8 Gy and 7.2 Gy, respectively, compared to 9.2 Gy and 7.7 Gy under static anatomy.

C. Computational Time and Memory Requirements

The major computational effort required in the preprocessing step (offline stage) of the proposed method is to pre-calculate per aperture and phase dose volumes. In this study, dose volumes were obtained using a previously developed Monte Carlo calculation engine *gPenelope*. Using this GPU-based calculation platform, dose for each combination of aperture and phase was obtained within approximately 0.5 minutes. Hence, the calculation of 1200 per aperture and phase dose volumes required approximately 10 hours to complete. Likewise, the deformable image registration and dose warping between 4D-CT phases and the reference CT can be performed prior to treatment. Using the deformation vector fields obtained from 4D-CT registration, it took approximately 1.6 hours to warp 1200 per aperture and phase dose volumes to the reference CT. Once the preprocessing step is completed, the proposed dose calculation scheme relies only on retrieving the instantaneously relevant warped dose volume from the memory based on current aperture and observed phase.

At the time of treatment and upon receipt of each cine-MRI frame, the online stage of the proposed method involves anatomic mapping and rigid translation and aggregation of the retrieved dose volume. The major computational effort required in anatomic mapping is the deformable registration of the current cine-MRI frame to the reference frame in order to obtain the deformation vector field and, in turn, the surrogate motion signal. B-spline registration for cine-MRI images ran at 8.8 ± 2.0 ms per iteration. To achieve real-time performance, computation time for cine-MRI registration was limited to 200 ms, thus allowing for around 20 iterations to be performed on the hardware applied in this study. Better performance could be achieved per unit time by alternative hardware (e.g., GPU implementation). Dose volume translation, re-sampling and aggregation requires only linear operations performed voxel-by-voxel. A dose volume with 100^3 voxels would require on the order of $<$10 ms for these operations on a modest CPU. Finally, the memory usage in the online stage of the proposed method is dominated by the memory required to load the pre-computed dose volumes. Assuming 1200 per aperture and phase dose volumes, each with 10^6 voxels conservatively containing double-precision floating-point numbers, approximately 10 GB of volatile memory - a modest value in terms of cost - would be required for loading data during treatment.

IV. DISCUSSION

In this note, the proposed dose accumulation model is used to compare the dosimetric impact of different delivery strategies. Results show that for the liver case tested in this study, dose delivery using free-breathing versus respiration-gated strategies could lead to dose discrepancy in CTV D_{98} and D_{min} up to 5% and 7%, respectively. While the example illustrated in this note is based on retrospective analysis of delivery strategies, the approach is primarily intended for real-time estimation of accumulated dose to potentially support dynamic, closed-loop plan re-optimization. To achieve such a scheme, the estimated cumulative dose can be implemented as a feedback signal to continuously monitor the progression of radiation delivery for any potential dose discrepancy due to anatomical variation. If necessary, real-time adjustments could then be made to the initial plan to correct the dose trajectory.

Dosimetric uncertainties in the proposed method predominantly stem from deviations between anatomy at the time of CT simulation and treatment. To mitigate such potential error, we apply rigid corrections for both target baseline shifts and out-of-range motion. While these corrections support more accurate intra-fractional modeling of the target motion, certain normal-tissue shape and position may vary unpredictably relative to CT simulation (e.g., peristalsis) and the proposed technique is not well-equipped to correct for such intra-fractional changes. Nonetheless, the proposed techniques could potentially be adapted to alternative imaging modalities (e.g., 4D-MRI) that could be acquired just prior to a treatment session. Another potential source of dosimetric uncertainty in the proposed method is due to the geometric inaccuracies associated with deformable image registration. In particular, the accuracy of 2D cine-MRI registrations employed in anatomic mapping was estimated to be 2.2 ± 1.1 mm[13]. Additionally, geometric errors in deformation vector fields obtained from 4D-CT registrations may compromise the accuracy of the 4D-CT surrogate motion signal and dose volume warping. Prior studies on the accuracy of 4D-CT deformable registration have reported a range of 1–6 mm for the average absolute error along the SI direction[14].

V. CONCLUSION

We have presented an approach for dose accumulation using cine-MRI and 4D-CT images. The method relies on an online anatomic mapping scheme between motion surrogates derived from cine-MRI and 4D-CT data. The proposed approach presents a compromise between sim-

plistic strategies in the literature that are based on shifting the planned dose volume and advanced methods that calculate per aperture dose on varying anatomy. By precomputing per aperture and phase dose volumes and warping them to a reference volume, the computational burden for potential real-time application is significantly relaxed.

A possible extension of the proposed approach is to pre-calculate dose volumes per each individual beamlet and 4D-CT phase. The dose volume deposited from any desired aperture in a given 4D-CT phase can then be approximated in real time by retrieving and aggregating the pre-calculated dose volumes of individual beamlets that are exposed in that aperture. The proposed extension accommodates cases in which the aperture shapes may vary during radiation delivery such as in MLC tracking[15].

ACKNOWLEDGMENT

This research was funded in part by the National Science Foundation through Award #1662819.

CONFLICTS OF INTEREST

The authors have no conflicts to disclose.

AUTHOR CONTRIBUTIONS STATEMENT

All authors have contributed to the design and implementation of the research and the writing of the technical note.

REFERENCES

[1]E. D. Brandner, A. Wu, H. Chen, D. Heron, S. Kalnicki, K. Komanduri, K. Gerszten, S. Burton, I. Ahmed, and Z. Shou, "Abdominal organ motion measured using 4DCT," International Journal of Radiation Oncology* Biology* Physics **65**, 554–560 (2006).

[2]Y. Mutaf, C. Scicutella, D. Michalski, K. Fallon, E. Brandner, G. Bednarz, and M. Huq, "A simulation study of irregular respiratory motion and its dosimetric impact on lung tumors," Physics in Medicine & Biology **56**, 845 (2011).

[3]T. Bortfeld, S. B. Jiang, and E. Rietzel, "Effects of motion on the total dose distribution," in *Seminars in radiation oncology*, Vol. 14 (Elsevier, 2004) pp. 41–51.

[4]K. Karlsson, I. Lax, E. Lindbäck, and G. Poludniowski, "Accuracy of the dose-shift approximation in estimating the delivered dose in SBRT of lung tumors considering setup errors and breathing motions," Acta Oncologica **56**, 1189–1196 (2017).

[5]S. Liu, T. R. Mazur, Y. Fu, H. H. Li, S. Mutic, and D. Yang, "A method to evaluate dosimetric effects on organs-at-risk for treatment delivery systematic uncertainties," Medical Physics **44**, 1552–1557 (2017).

[6]P. R. Poulsen, M. L. Schmidt, P. Keall, E. S. Worm, W. Fledelius, and L. Hoffmann, "A method of dose reconstruction for moving targets compatible with dynamic treatments," Medical Physics **39**, 6237–6246 (2012).

[7]B. Stemkens, M. Glitzner, C. Kontaxis, B. D. De Senneville, F. M. Prins, S. P. Crijns, L. G. Kerkmeijer, J. J. Lagendijk, C. A. Van Den Berg, and R. H. Tijssen, "Effect of intra-fraction motion on the accumulated dose for free-breathing MR-guided stereotactic body radiation therapy of renal-cell carcinoma," Physics in Medicine & Biology **62**, 7407 (2017).

[8]G. Sharp, R. Li, J. Wolfgang, G. Chen, M. Peroni, M. Spadea, S. Mori, J. Zhang, J. Shackleford, and N. Kandasamy, "Plastimatch-an open source software suite for radiotherapy image processing," in *Proceedings of the XVI'th International Conference on the use of Computers in Radiotherapy (ICCR), Amsterdam, Netherlands* (2010).

[9]Y. Wang, T. R. Mazur, O. Green, Y. Hu, H. Li, V. Rodriguez, H. O. Wooten, D. Yang, T. Zhao, S. Mutic, *et al.*, "A GPU-accelerated monte carlo dose calculation platform and its application toward validating an MRI-guided radiation therapy beam model," Medical Physics **43**, 4040–4052 (2016).

[10]S. Mutic and J. F. Dempsey, "The ViewRay system: magnetic resonance–guided and controlled radiotherapy," Seminars in Radiation Oncology **24**, 196–199 (2014).

[11]M. Vallières, C. R. Freeman, S. R. Skamene, and I. El Naqa, "A radiomics model from joint FDG-PET and MRI texture features for the prediction of lung metastases in soft-tissue sarcomas of the extremities," Physics in Medicine & Biology **60**, 5471 (2015).

[12]A. T. Fernandes, S. Apisarnthanarax, L. Yin, W. Zou, M. Rosen, J. P. Plastaras, E. Ben-Josef, J. M. Metz, and B.-K. Teo, "Comparative assessment of liver tumor motion using cine-magnetic resonance imaging versus 4-dimensional computed tomography," International Journal of Radiation Oncology* Biology* Physics **91**, 1034–1040 (2015).

[13]G. Sharp, S. Mirzapourrezaei, T. Mazur, N. Kandasamy, J. Shackleford, and E. Salari, "Real-time deformable image registration for MRI-guided radiotherapy," in *Proceedings of the 104th Scientific Assembly and Annual Meeting of the Radiological Society of North America (RSNA), Chicago, IL* (2018).

[14]K. K. Brock and Deformable Registration Accuracy Consortium, "Results of a multi-institution deformable registration accuracy study (MIDRAS)," International Journal of Radiation Oncology* Biology* Physics **76**, 583–596 (2010).

[15]M. Glitzner, P. Woodhead, P. Borman, J. Lagendijk, and B. Raaymakers, "MLC-tracking performance on the Elekta Unity MRI-linac," Physics in Medicine & Biology **64**, 15NT02 (2019).

Figure captions

Fig 1: Steps of the proposed dose accumulation approach

Fig 2: The schematic for anatomic mapping of cine-MRI frames onto 4D-CT phases

Fig 3: Illustration of baseline-shift and out-of-range detection: (a) Baseline-shift detection on actual signal; (b) Out-of-range detection on detrended signal

Fig 4: Surrogate motion signal and rigid corrections for the liver cancer case: (a) Sample cine-MRI signal and the calculated baseline drift; (b) and (c) Histograms of the applied baseline-shift and out-of-range corrections, respectively, over all three fractions

Fig 5: 4D-CT phase labeling for fraction 1 of the liver case using the anatomic mapping procedure: (a) Histogram of SI displacements obtained from the detrended motion signal; (b) Histogram of 4D-CT phase labels

Fig 6: Comparing DVH of cumulative dose under different delivery strategies for fraction 1 of the liver case

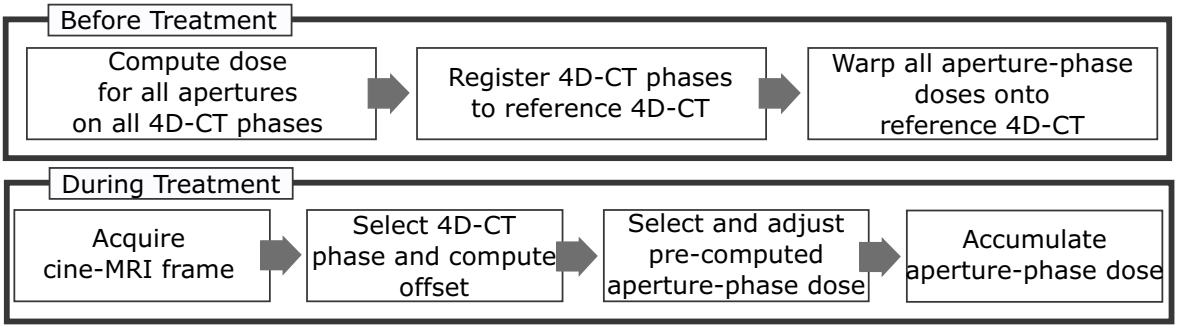

FIG. 1: Steps of the proposed dose accumulation approach

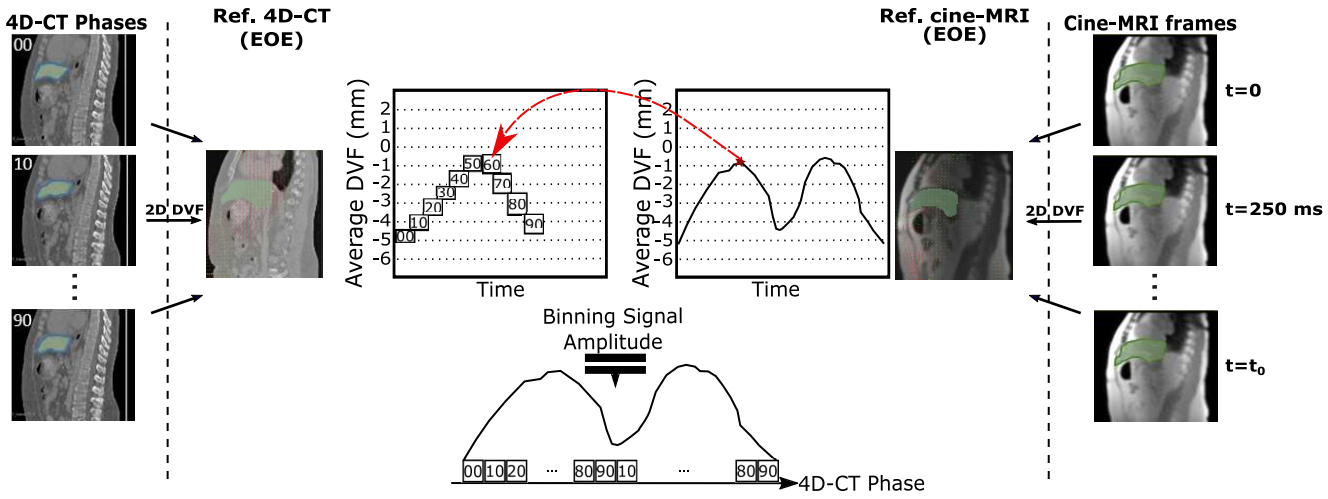

FIG. 2: The schematic for anatomic mapping of cine-MRI frames onto 4D-CT phases

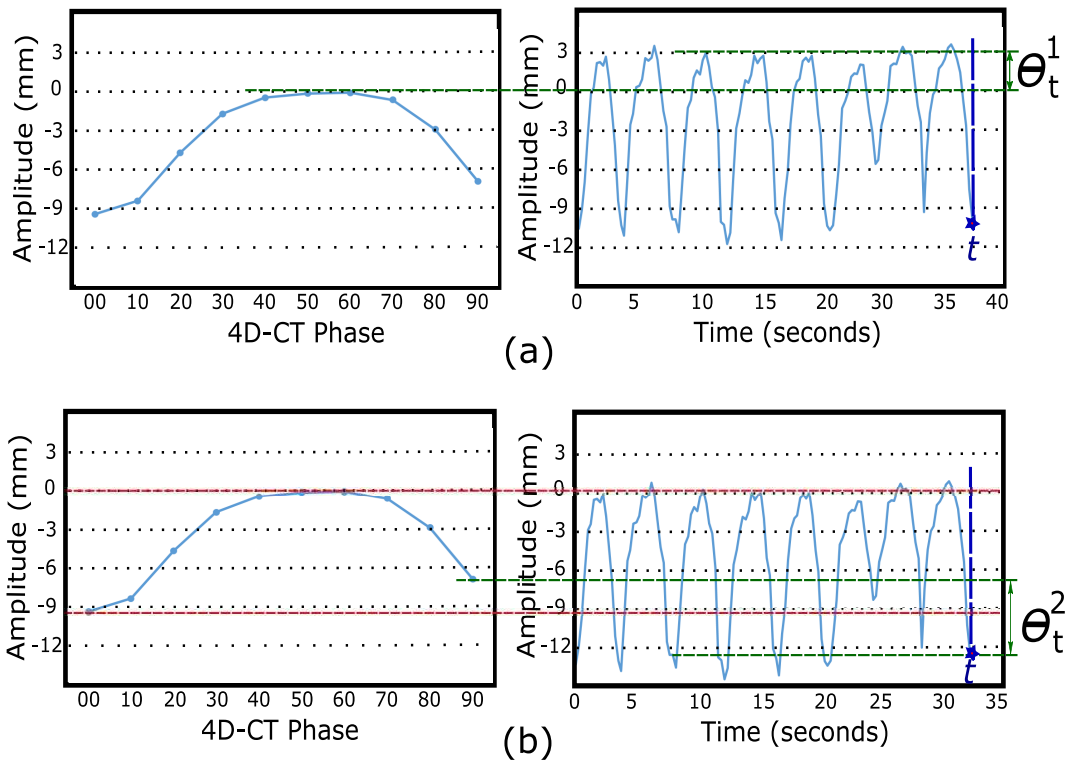

FIG. 3: Illustration of baseline-shift and out-of-range detection: (a) Baseline-shift detection on actual signal; (b) Out-of-range detection on detrended signal

Algorithm 1 Real-time dose accumulation

$\mathbf{d}^{\text{cum}} \leftarrow \mathbf{0}$

for $t = 1 : T$ **do**

Calculate signal amplitude x_t from acquired cine-MRI frame

Calculate detrended signal amplitude x_t^D

Calculate moving average velocity of signal $\bar{v}_t$

Select best-matching 4D-CT phase ϕ_t using x_t^D and $\bar{v}_t$

Identify index of current aperture a_t

Retrieve warped dose volume $\mathbf{d}_{(a_t,\phi_t)}$

Calculate offset $\theta_t = \theta_t^1 + \theta_t^2$

Perform rigid translation of $\mathbf{d}_{(a_t,\phi_t)}$ by offset θ_t to obtain $\bar{\mathbf{d}}_{(a_t,\phi_t)}$

$\mathbf{d}^{\text{cum}} \leftarrow \mathbf{d}^{\text{cum}} + \bar{\mathbf{d}}_{(a_t,\phi_t)}$

end for

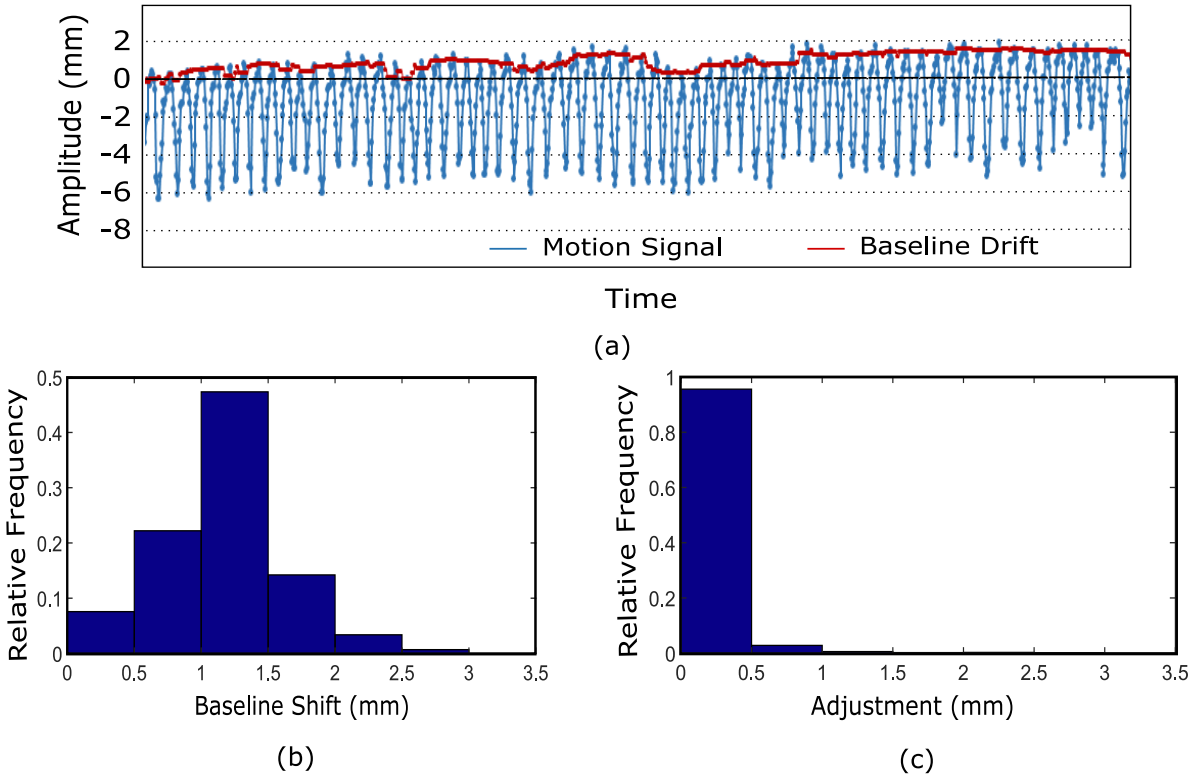

FIG. 4: Surrogate motion signal and rigid corrections applied for the liver cancer case: (a) Sample cine-MRI signal and the calculated baseline drift; (b) and (c) Histograms of the applied baseline-shift and out-of-range corrections, respectively, over all three fractions

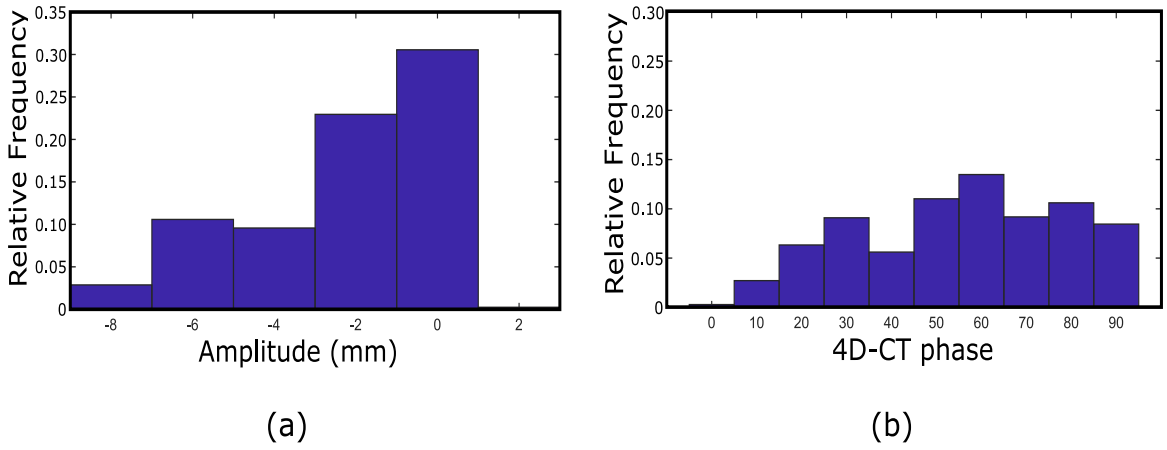

FIG. 5: 4D-CT phase labeling for fraction 1 of the liver case using the anatomic mapping procedure: (a) Histogram of SI displacements obtained from the detrended motion signal; (b) Histogram of 4D-CT phase labels

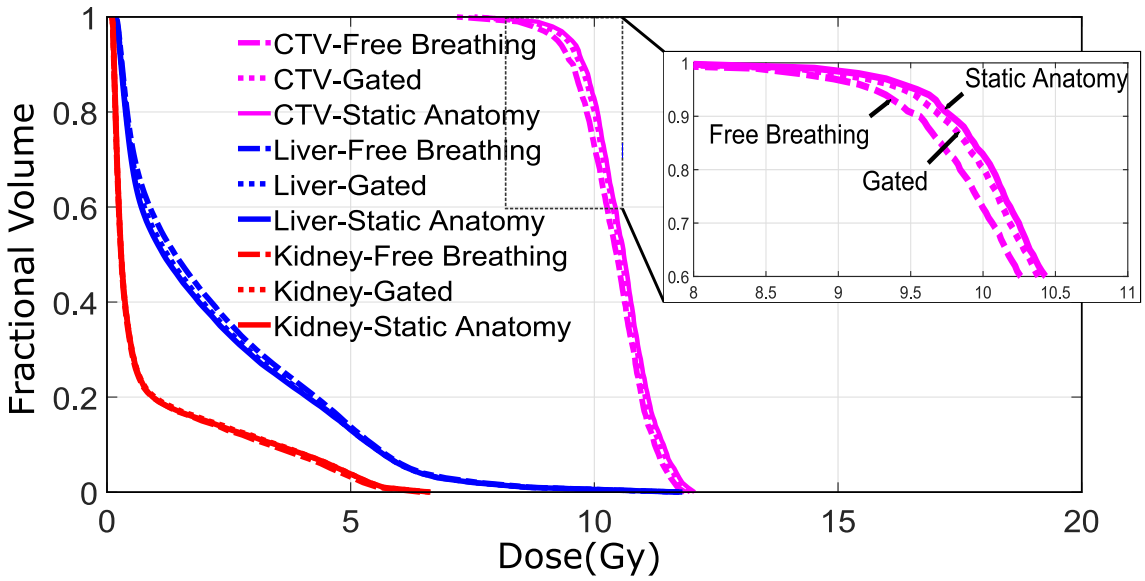

FIG. 6: Comparing DVH of cumulative dose under different delivery strategies for fraction 1 of liver case

TABLE I: DVH metrics for CTV, healthy liver, and kidneys calculated for different fractions of the liver case

		CTV		Liver	Kidneys
		D_{98} (Gy)	D_{min} (Gy)	D_{mean} (Gy)	D_{mean} (Gy)
Planned dose (static anatomy)		9.16	7.71	2.13	0.92
Fraction #	**Scenario**				
1	**Free breathing**	8.76	7.20	2.26	0.93
	Gated	9.00	7.56	2.16	0.90
2	**Free breathing**	8.90	7.43	2.19	0.95
	Gated	9.02	7.66	2.13	0.92
3	**Free breathing**	8.84	7.37	2.20	0.97
	Gated	9.09	7.77	2.08	0.92